THE ASTROPHYSICAL JOURNAL, 413:611–618, 1993 August 20

EMISSION OF HeH^+ IN NEBULAE

C. CECCHI-PESTELLINI[1] AND A. DALGARNO
Harvard-Smithsonian Center for Astrophysics, Cambridge, MA 02138
Received 1992 December 10; accepted 1993 February 25

ABSTRACT

The formation and destruction processes of HeH^+ in nebulae are discussed, and calculations of the abundances of HeH^+ are presented. It is shown that for effective temperatures of the ionizing source exceeding 50,000 K, the abundances are of the order of 10^{12} cm^{-2}, largely independent of the nebular parameters. The emission-line intensities increase approximately as the density of the nebula. Results are given for two detailed models of the planetary nebula NGC 7027. The predicted intensities exceed the observational upper limit. The emissions have sharply peaked distributions with maximum intensity reached in a narrow zone at the edge of the ionized region. The greater part of the emission may be outside the region observed.

Subject headings: ISM: abundances — molecular processes — planetary nebulae: individual (NGC 7027)

1. INTRODUCTION

Moorhead et al. (1988) conducted a careful search for emission from the molecular ion HeH^+ in the spectrum of the planetary nebula NGC 7027 and found no evidence of it, contrary to expectation based on the discussion of the formation and destruction mechanisms by Roberge & Dalgarno (1982b). The possibility that the rate coefficient of a major formation mechanism,

$$He^+ + H \rightarrow HeH^+ + h\nu \,, \qquad (1)$$

had been overestimated (Moorhead et al. 1988) by Roberge & Dalgarno (1982b) has been eliminated by the accurate calculations of Zygelman & Dalgarno (1990), who obtained values larger than those adopted in the earlier discussion.

We employ here a more comprehensive chemistry of HeH^+ in ionized plasmas, and we explore the dependence of the abundances on nebular parameters. The emission from NGC 7027 is discussed.

2. THE IONIZATION STRUCTURE

The formation of HeH^+ depends on the ionization structure of the nebula and in particular on the overlap of ionized and neutral material. We assume spherical, static nebulae in thermal and ionization equilibrium. The central stars of planetary nebulae radiate energetic photons that may doubly ionize helium to produce an inner zone of He^{2+}. Recombination of He^{2+} to He^+ is accompanied by the emission of photons that ionize hydrogen, and no HeH^+ can be produced in this inner zone. We assume that all photons energetically capable of producing He^{2+} are fully absorbed in the central region, although for the hotter stars the assumption is not strictly valid. The ionization structure of the surrounding plasma can be determined by solving the ionization equations for H and He in a radiation field with frequencies lying between the ionization threshold ν_1 of H and the ionization threshold $4\nu_1$ of He^+.

To solve the radiative transfer problem, we adopted the on-the-spot approximation in which the hydrogen resonance recombination radiation is immediately reabsorbed by hydrogen, and the helium recombination by helium. The approximation leads to considerable simplification, and it provides a satisfactory representation of the ionization distribution in a dust-free nebula (Hummer & Seaton 1963, 1964; Rubin 1984). When dust is present, a generalized on-the-spot approximation is needed which allows for the absorption of the diffuse radiation by dust (Petrosian & Dana 1975; Sarazin 1977). To describe the dust absorption, we used an effective cross section

$$\sigma_g(\nu) = 0.47 \times 10^{-21}(A_\nu/A_v) \text{ cm}^2 \,, \qquad (2)$$

where A_ν is the extinction at frequency ν, expressed in magnitudes. We adopted the values of A_ν calculated by Draine & Lee (1984) and discussed by Roberge (1990) and Roberge et al. (1991).

In calculating the distributions of H^+ and He^+ through the nebula, we took the coupled equations in the form given by Tielens & de Jong (1979) and solved them with the Bulirsh-Stoer method.

We characterized the stellar radiation field by its luminosity Q_H in photons able to ionize atomic hydrogen and by a blackbody spectral distribution at a temperature T^* with a high-frequency cutoff consistent with the selected value of Q_H.

Figures 1*a*–1*d* show the results in the form of the distributions of the neutral atoms H and He for $Q_H = 1 \times 10^{48}$ s^{-1}, $n_H = 10^4$ cm^{-3}, $n_{He} = 10^3$ cm^{-3}, and $T^* = 25{,}000$, 50,000, 100,000, and 200,000 K in dust-free plasmas, and Figures 2*a*–2*d* give the results for plasmas with a dust content like that of the average interstellar medium. As the stellar temperature increases and the high-frequency flux steepens, the He^+ zone grows to equal and then slightly exceed the H^+ zone, and for T^* above 50,000 K there is a region in which He^+ ions overlap with neutral hydrogen atoms and conditions are conducive to the formation of HeH^+. The inclusion of dust reduces the extent of the ionized zones as the dust absorbs some of the ionizing radiation.

3. CHEMISTRY OF HeH^+

The molecular ion HeH^+ may be formed by reaction (1) (Roberge & Dalgarno 1982b). The rate coefficient has a value of 1×10^{-15} cm^3 s^{-1} between 2000 and 10,000 K (Zygelman & Dalgarno 1990). Additional sources are the radiative association of H^+ and He,

$$H^+ + He \rightarrow HeH^+ + h\nu \,; \qquad (3)$$

[1] Permanent address: Dipartimento di Astronomia e Scienza dello Spazio, Università degli Studi, Largo Enrico Fermi 5, 50125 Firenze, Italy.

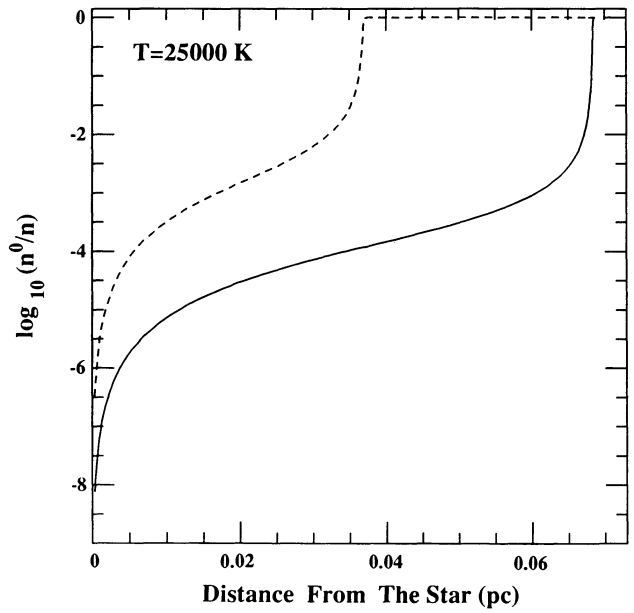

FIG. 1*a*

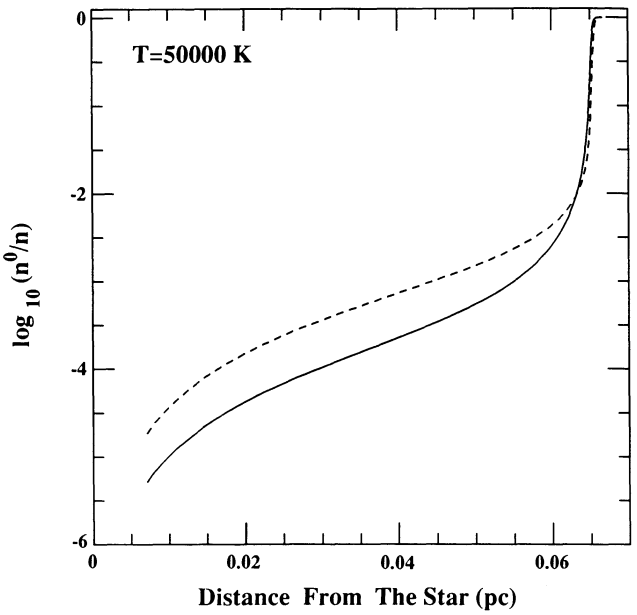

FIG. 1*b*

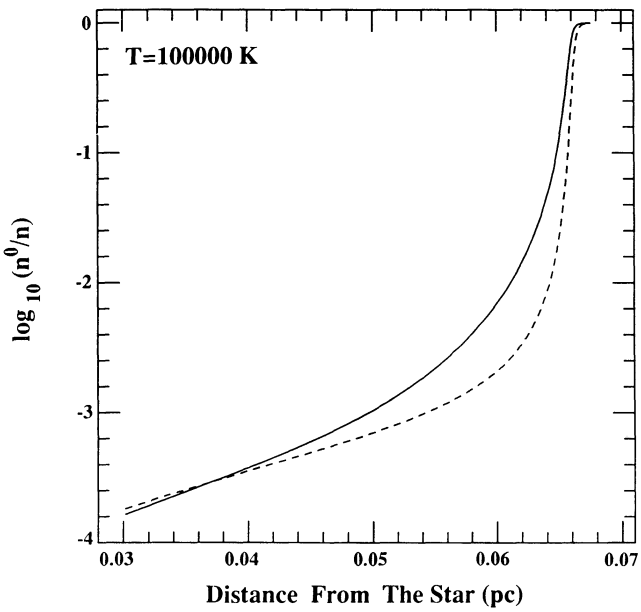

FIG. 1*c*

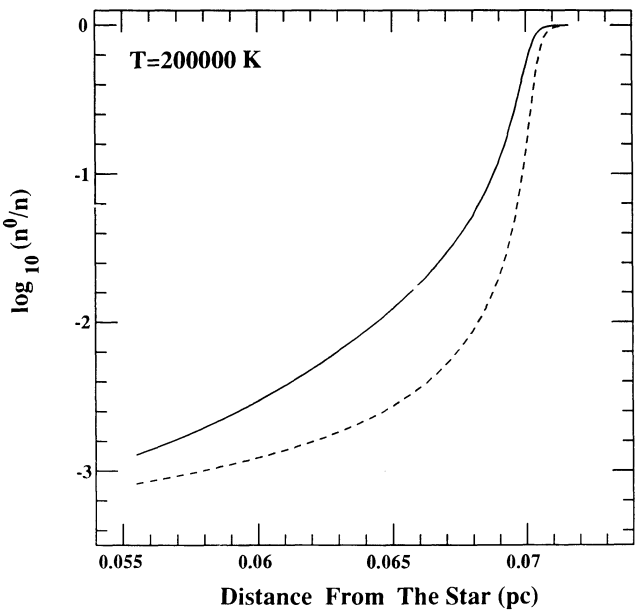

FIG. 1*d*

FIG. 1.—Distribution of neutral hydrogen (*solid curve*) and neutral helium (*dashed curve*) for T^* equal to (*a*) 25,000 K, (*b*) 50,000 K, (*c*) 100,000 K, and (*d*) 200,000 K in a dust-free plasma with $n_H = 10^4$ cm^{-3}, $n_{He} = 10^3$ cm^{-3}, and $Q_H = 1 \times 10^{48}$ s^{-1}.

associative ionization of H and of H_2 with metastable helium He*,

$$He^* + H \rightarrow HeH^+ + e\,, \tag{4}$$

$$He^* + H_2 \rightarrow HeH^+ + H + e\,; \tag{5}$$

and reactions with vibrationally excited H_2^+ ions,

$$H_2^+ + He \rightarrow HeH^+ + H\,. \tag{6}$$

The rate coefficients have been listed by Roberge & Dalgarno (1982b).

The H_2^+ and H_2 molecular species are formed by

$$H + H^+ \rightarrow H_2^+ + h\nu\,, \tag{7}$$

$$H_2^+ + H \rightarrow H_2 + H^+\,, \tag{8}$$

$$H + e \rightarrow H^- + h\nu\,, \tag{9}$$

$$H^- + H \rightarrow H_2 + e\,. \tag{10}$$

The rate coefficients have been listed by Dalgarno & Lepp (1985). In a dusty plasma, H_2 may also be formed by grain

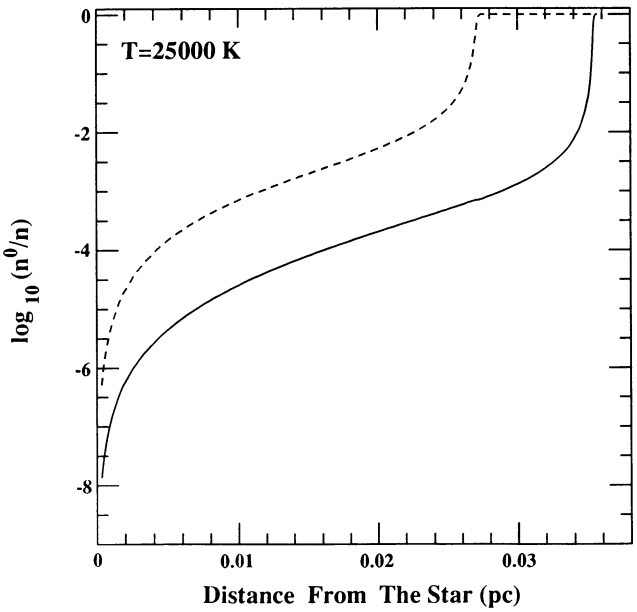

FIG. 2*a*

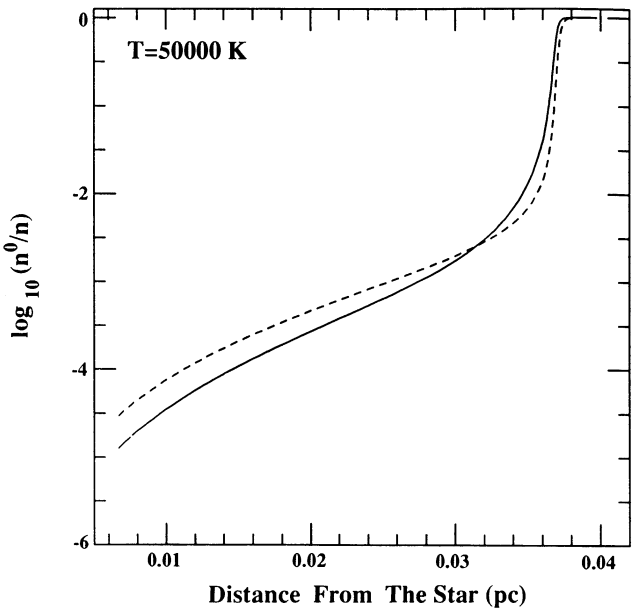

FIG. 2*b*

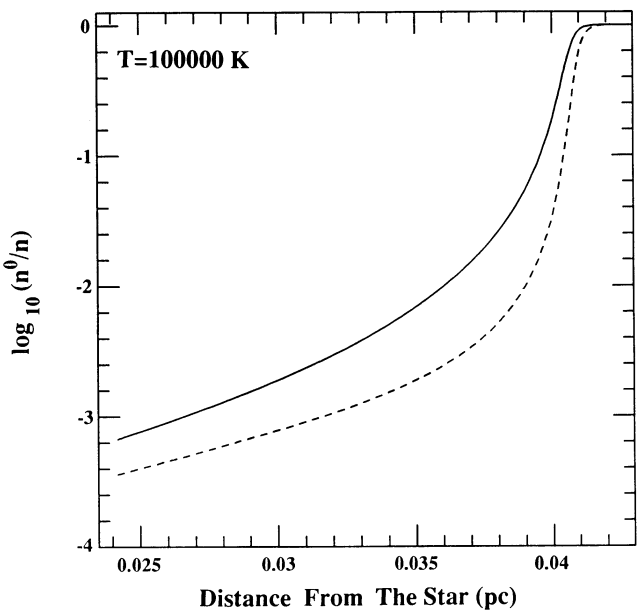

FIG. 2*c*

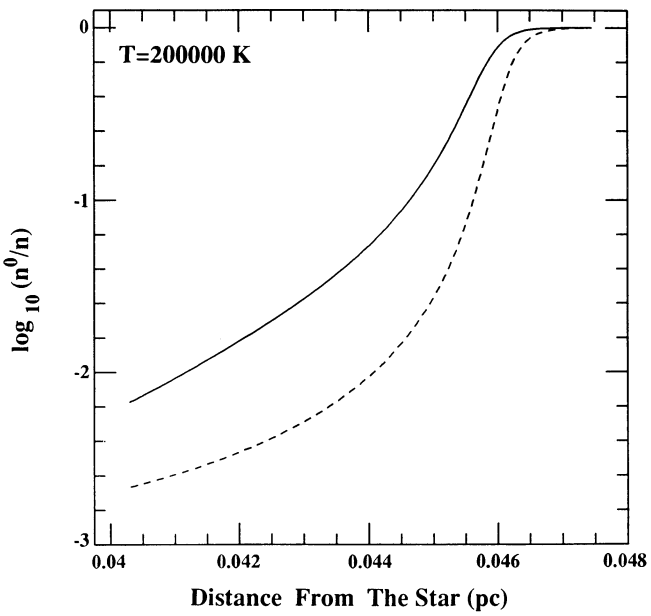

FIG. 2*d*

FIG. 2.—Same as Fig. 1, but for a plasma with dust

catalysis,

$$H + H_g \rightarrow H_2 + g \, . \tag{11}$$

We adopted a rate of $3 \times 10^{-17} n_H \, s^{-1}$.

The negative H^- ions can be lost by mutual neutralization:

$$H^+ + H^- \rightarrow H + H \, , \tag{12}$$

$$He^+ + H^- \rightarrow He + H \, , \tag{13}$$

$$H_2^+ + H^- \rightarrow H_2 + H \, , \tag{14}$$

and by photodetachment,

$$H^- + h\nu \rightarrow H + e \, . \tag{15}$$

The molecular ion H_2^+ is removed by dissociative recombination,

$$H_2^+ + e \rightarrow H + H \, , \tag{16}$$

and by photodissociation,

$$H_2^+ + h\nu \rightarrow H + H^+ \, . \tag{17}$$

The molecular hydrogen is removed by photodissociation,

$$H_2 + h\nu \rightarrow H + H \, ; \tag{18}$$

by photoionization,

$$H_2 + h\nu \rightarrow H_2^+ + e \tag{19}$$

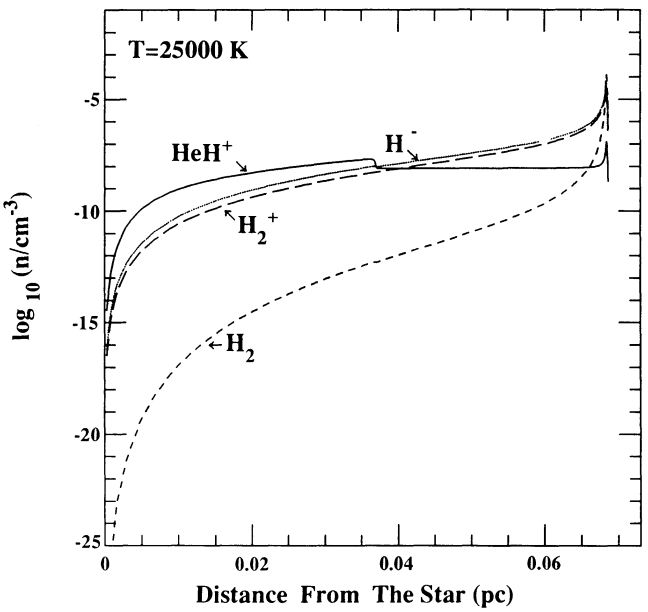

FIG. 3*a*

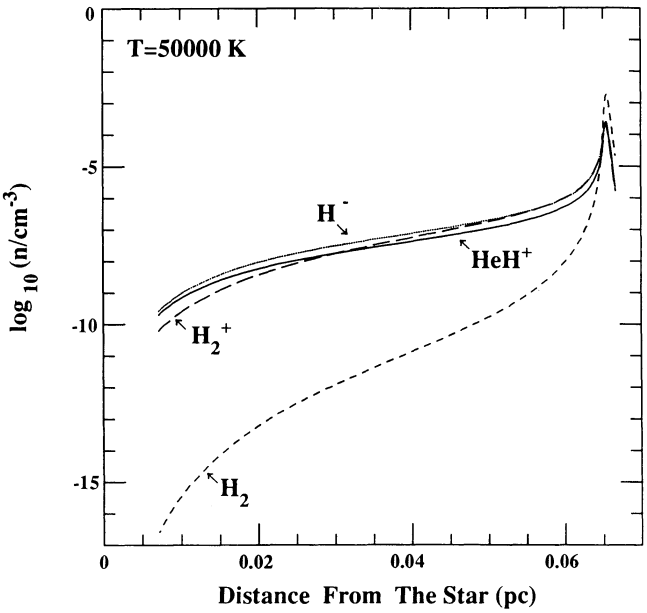

FIG. 3*b*

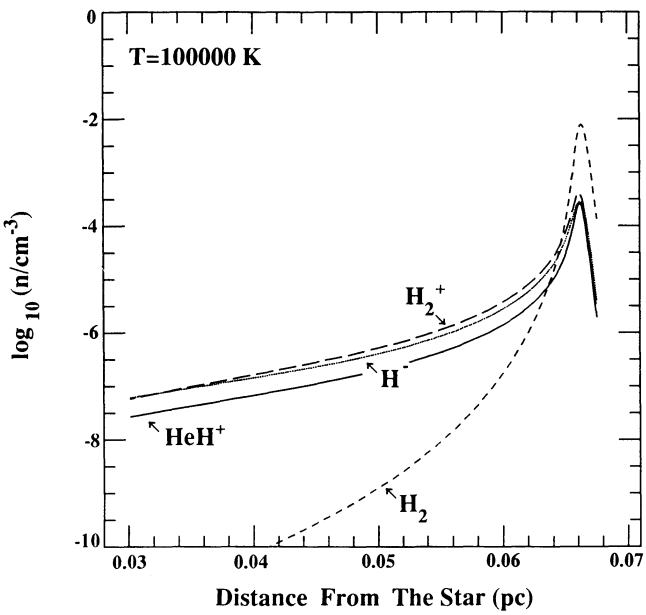

FIG. 3*c*

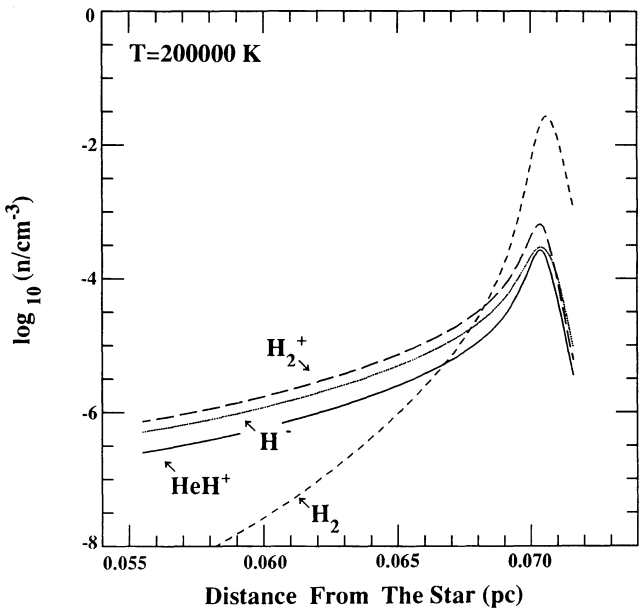

FIG. 3*d*

FIG. 3.—Concentrations of neutral and ionized species for the conditions of Figs. 1*a*–1*d*

(O'Neill & Reinhardt 1978; Kossman et al. 1989); and by reaction with He^+,

$$He^+ + H_2 \rightarrow He + H + H^+ , \quad (20)$$

which is rapid for H_2 in vibrational levels $v \geq 2$ (Jones et al. 1986). H_2 can also be removed by reactions with minor species. The reaction

$$C^+ + H_2 \rightarrow CH^+ + H \quad (21)$$

is also rapid if H_2 is vibrationally excited (Jones et al. 1986).

Direct collision-induced dissociations,

$$H + H_2 \rightarrow H + H + H , \quad (22)$$

$$He + H_2 \rightarrow He + H + H , \quad (23)$$

occur (Roberge & Dalgarno 1982a; Lepp & Shull 1983; Dove & Mandy 1986; Dove et al. 1987).

The main removal mechanisms for HeH^+ are dissociative recombination,

$$HeH^+ + e \rightarrow He + H ; \quad (24)$$

photodissociation,

$$HeH^+ + h\nu \rightarrow He + H^+ ; \quad (25)$$

and reactions with atomic hydrogen,

$$HeH^+ + H \rightarrow H_2^+ + He , \quad (26)$$

with molecular hydrogen,

$$HeH^+ + H_2 \rightarrow H_3^+ + He , \quad (27)$$

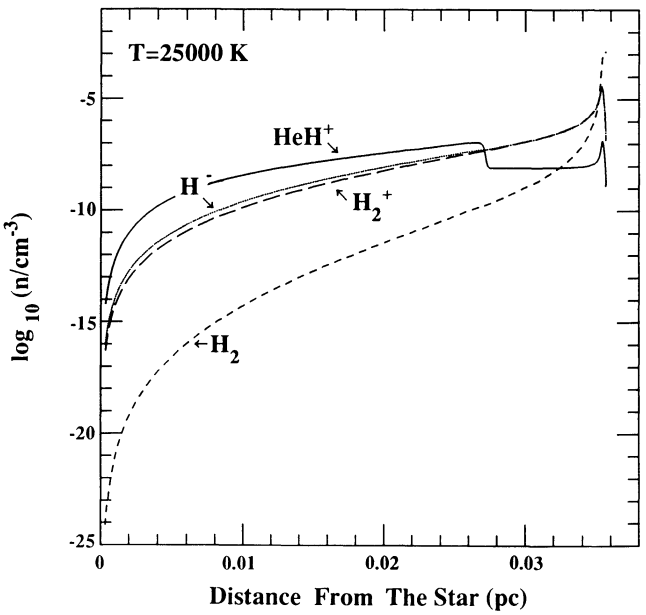

FIG. 4*a*

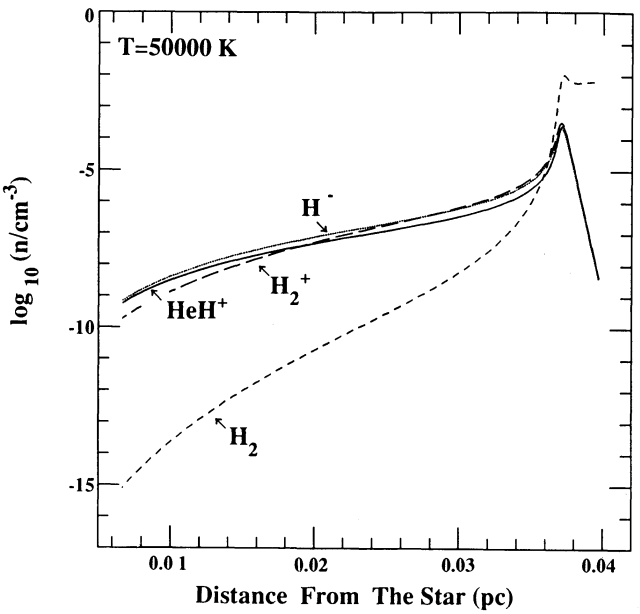

FIG. 4*b*

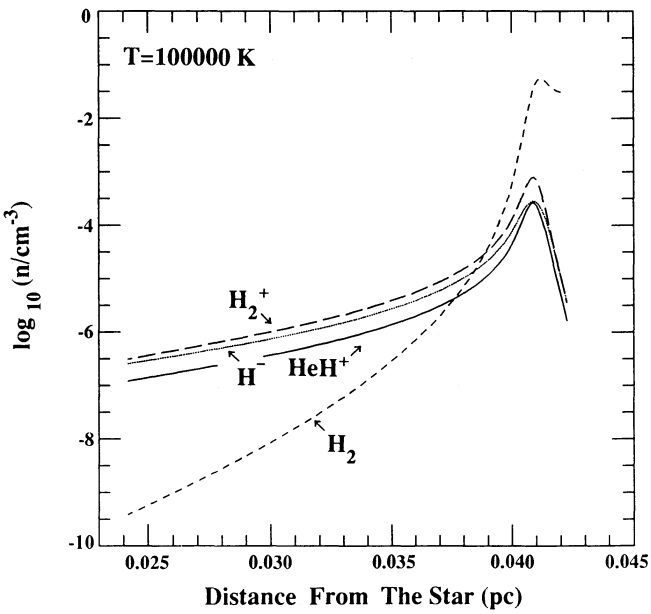

FIG. 4*c*

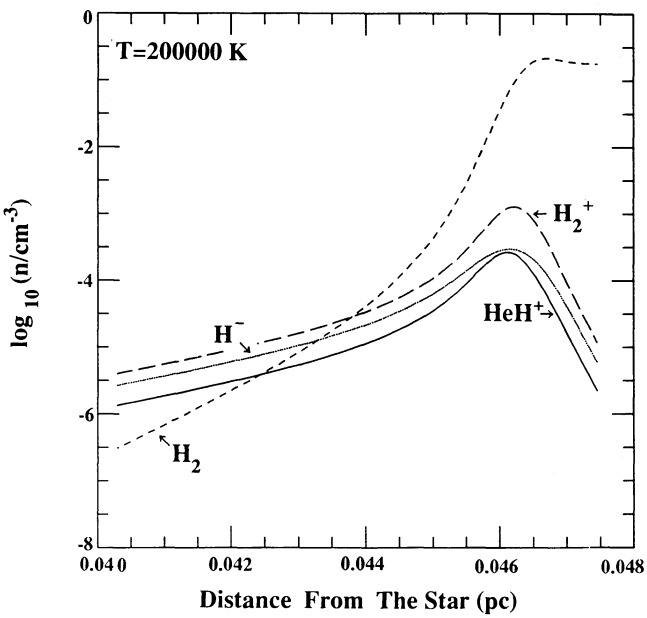

FIG. 4*d*

FIG. 4.—Concentrations of neutral and ionized species for the conditions of Figs. 2*a*–2*d*

and with H^-,

$$HeH^+ + H^- \rightarrow He + H + H \,. \quad (28)$$

Collision-induced dissociation,

$$H + HeH^+ \rightarrow H + He + H^+ \,, \quad (29)$$

may be effective in weakly ionized plasmas.

Of major importance is the dissociative recombination reaction (24). The process was predicted to be slow (Roberge & Dalgarno 1982b; Michels 1989) because of the inaccessibility of suitable potential energy curves, but experiments (Yousif & Mitchell 1989) yield a rate coefficient of $2 \times 10^{-8}\ (300/T)^{1/2}$ $cm^3\ s^{-1}$ which, though smaller than commonly occurs, is large enough that dissociative recombination is a major destruction mechanism.

4. THE ABUNDANCES OF HeH^+

We have solved numerically the set of chemical rate equations and obtained the concentrations of the various species as functions of distance from the central star. Some examples are presented in Figures 3*a*–3*d* and 4*a*–4*d* for the same conditions as in Figures 1 and 2. For stellar temperatures above 50,000 K, the major source of HeH^+ is reaction (1), the radiative association of He^+ and H. The principal destruction mechanisms are photodissociation (reaction [25]) close to the star, dissociative recombination (reaction [24]) in the intermediate region, and

reaction with atomic hydrogen (reaction [26]) in the outer zone.

The peak value of the HeH^+ density is largely independent of the stellar radiation field. The distance of the peak from the central ionizing source moves from 0.065 to 0.073 pc as T^* increases from 50,000 to 300,000 K for a density of 10^4 cm^{-3} and $Q_H = 1 \times 10^{48}$ s^{-1}, but the maximum density remains close to 2.6×10^{-4} cm^{-3}.

Inside the location where the HeH^+ concentration obtains its maximum value, the destruction of HeH^+ by dissociative recombination increases rapidly with the rising fractional ionization. Beyond the peak, the destruction of HeH^+ by reaction with neutral atomic hydrogen also increases rapidly as the neutral fraction of hydrogen approaches unity. The region over which the transition occurs is very narrow, so that the peak occurs where the two destruction mechanisms are comparable.

Beyond the peak, $n(HeH^+) \sim 10^{-5} n(He^+)$ and inside the peak $n(HeH^+) \sim 2 \times 10^{-7} n(H) n(He^+)/n_e$, so that the abundance of HeH^+ is controlled by the distribution of ionization between hydrogen and helium. The peak occurs where the neutral hydrogen fraction is about 0.98, and the outer extent of the HeH^+ region is determined by the size of the He^+ zone.

The magnitude of the peak is proportional to the density of He^+. In Figures 5 and 6 we show the concentrations of HeH^+ for densities of 10^4, 10^5, and 10^6 cm^{-3} for $T^* = 150{,}000$ K and $Q_H = 10^{47}$ s^{-1} in a nebula without and with dust. The distances are shown as ratios to the Strömgren radius R_S.

The calculated column densities $N(HeH^+)$ of HeH^+ integrated through the nebula for which the ionizing flux $Q_H = 10^{48}$ s^{-1}, the hydrogen density $n_H = 10^4$ cm^{-3}, and the helium-to-hydrogen ratio y is equal to 0.1 are presented for nebulae without and with dust in Table 1.

The column densities increase abruptly at $T^* = 50{,}000$ K as the ionized helium zone moves out to match the ionized hydrogen zone, creating a region of overlap of H and He^+. Above

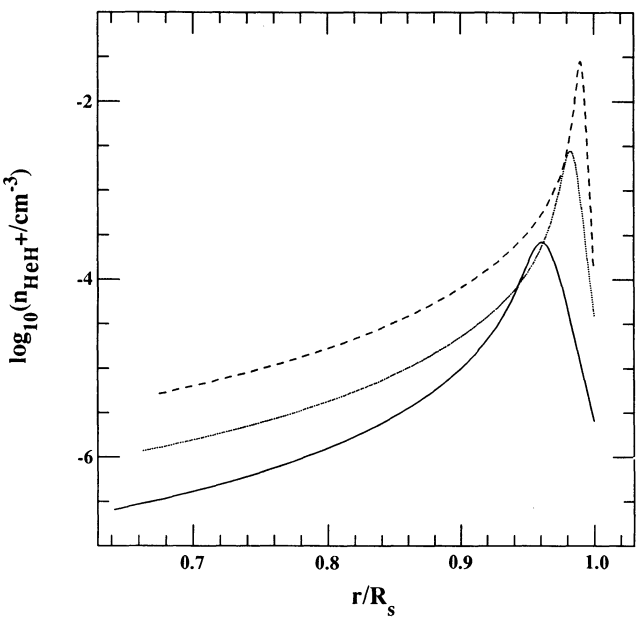

FIG. 5.—Concentrations of HeH^+ for hydrogen densities of 10^4 cm^{-3} (*solid curve*), 10^5 cm^{-3} (*dotted curve*), and 10^6 cm^{-3} (*dashed curve*) for a dust-free plasma with $T^* = 150{,}000$ K and $Q_H = 10^{47}$ s^{-1}.

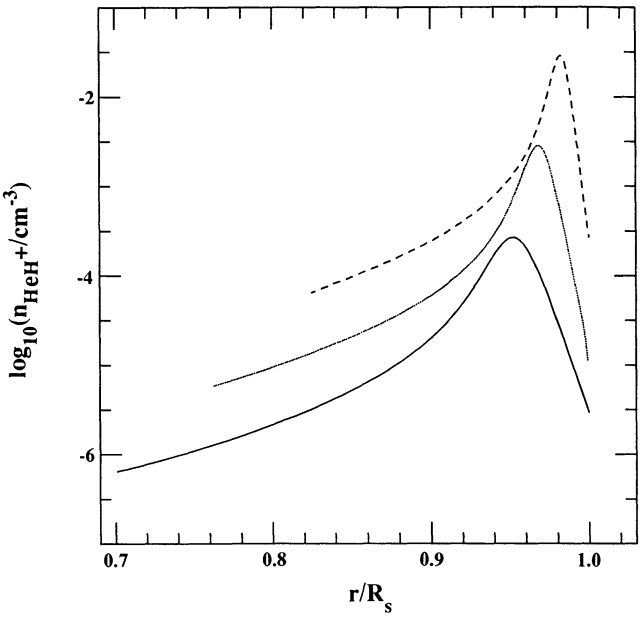

FIG. 6.—Same as Fig. 5, but for a plasma with dust

100,000 K the column densities vary little. They are of the order 10^{12} cm^{-2}, the values in the dust-free nebulae being slightly larger. The dependence of $N(HeH^+)$ on n_H and Q_H is illustrated in Table 2 for $T^* = 150{,}000$ K and $y = 0.1$. The column densities show a small increase with density and with ionizing flux.

The insensitivity of the column densities to the density n_H arises because the increases in the peak concentration of HeH^+ shown in Figure 5 are countered by a decrease in the width of the HeH^+ zone which is controlled by the optical depth of the ionizing photons. The insensitivity to Q_H and to T^* above 50,000 K occurs because the production of HeH^+ is determined by the overlap of a neutral component H with the ionized component He^+, and the distribution of ionization

TABLE 1

COLUMN DENSITIES $N(HeH^+)$[a] IN A NEBULA WITHOUT AND WITH DUST

	T^* (K)					
	25,000	50,000	100,000	150,000	200,000	300,000
Without dust	0.02	5.3	8.5	9.1	9.2	9.0
With dust	0.02	5.0	8.3	8.8	8.7	8.3

[a] In 10^{11} cm^{-2} for $Q_H = 10^{48}$ s^{-1}, $n_H = 10^4$ cm^{-3}, and $y = 0.1$.

TABLE 2

COLUMN DENSITIES $N(HeH^+)$[a] IN A DUST-FREE NEBULA

	Q_H (s^{-1})		
n_H (cm^{-3})	10^{47}	10^{48}	10^{49}
10^4	8.3	9.1	10.0
10^5	9.5	10.3	11.2
10^6	10.5	11.2	12.0

[a] In 10^{11} cm^{-2} for $T^* = 150{,}000$ K and $y = 0.1$.

between hydrogen and helium does not depend on the absolute values of the ionizing flux.

The predicted abundances of HeH^+, then, for any star hotter than 50,000 K are 10^{12} cm^{-2}.

The intensities of the emission lines of HeH^+ do increase with density because they are determined by the integral of the product of n_e and $n(HeH^+)$, provided that n_e is not so large that the excited states are quenched. The critical electron density for vibrational quenching is 10^{11} cm^{-3}, so that each excitation to the $v = 1$ level is followed by emission. The critical density for rotational quenching in the ground vibrational state is about 10^7 cm^{-3} for the $j = 1$ rotational level and larger for the higher rotational levels. If the electron density is smaller than 10^6 cm^{-3}, the HeH^+ molecules reside mostly in the $j = 0$ level, from which electron impacts cause excitation to the $j = 1$ levels of the $v = 0$ and $v = 1$ vibrational states, resulting in emission at 149.13, 3.364 and 3.608 μm.

The column emission intensities of the pure rotational line at 149.13 μm is given by

$$F_v = h\nu \int q^r_{01}\, n_e\, n(HeH^+) d\ell \text{ ergs cm}^{-2}\text{ s}^{-1}, \quad (30)$$

where ν is the the line frequency, q^r_{01} is the rate coefficient for rotational excitation, and the integral over the line of sight extends through the nebula. For the two rovibrational lines from $v = 1$ at $\lambda_1 = 3.364$ μm and $\lambda_2 = 3.608$ μm, the column emission intensities are given by

$$F_{\nu_i} = \frac{h\nu_i A_i}{A_1 + A_2} \int n_e\, n(HeH^+) q^v_{01}\, d\ell \text{ ergs cm}^{-2}\text{ s}^{-1}, \quad (31)$$

where A_i is the transition probability of the line with wavelength λ_i and frequency ν_i, and q^v_{01} is the rate coefficient for vibrational excitation.

Table 3 lists the intrinsic column emission intensities for the conditions adopted for Table 2, calculated using a rate coefficient for vibrational excitation $q^v_{01} = 3.3 \times 10^{-9}$ cm^3 s^{-1} and a rate coefficient for rotational excitation $q^r_{01} = 4 \times 10^{-7}$ cm^3 s^{-1}. The intensities increase at a rate nearly proportional to the density.

TABLE 3

INTRINSIC COLUMN EMISSION INTENSITIES F_ν (ergs cm^{-2} s^{-1})

n_H (cm^{-3})	Q_H (s^{-1})	Dust-free	With Dust
		3.364 μm	
10^4	10^{47}	1.7×10^{-6}	1.6×10^{-6}
	10^{48}	2.0×10^{-6}	1.9×10^{-6}
	10^{49}	2.4×10^{-6}	2.1×10^{-6}
10^5	10^{47}	2.2×10^{-5}	2.0×10^{-5}
	10^{48}	2.5×10^{-5}	2.2×10^{-5}
	10^{49}	2.9×10^{-5}	2.3×10^{-5}
10^6	10^{47}	2.5×10^{-4}	2.2×10^{-4}
	10^{48}	2.9×10^{-4}	2.4×10^{-4}
	10^{49}	3.3×10^{-4}	2.4×10^{-4}
		3.609 μm	
10^4	10^{47}	3.6×10^{-6}	3.4×10^{-4}
	10^{48}	4.3×10^{-6}	3.9×10^{-4}
	10^{49}	5.0×10^{-6}	4.4×10^{-4}
10^5	10^{47}	4.5×10^{-5}	4.1×10^{-5}
	10^{48}	5.2×10^{-5}	4.5×10^{-5}
	10^{49}	6.0×10^{-5}	4.8×10^{-5}
10^6	10^{47}	5.3×10^{-4}	4.6×10^{-4}
	10^{48}	6.0×10^{-4}	4.9×10^{-4}
	10^{49}	6.9×10^{-4}	5.1×10^{-4}
		149.13 μm	
10^4	10^{48}	1.8×10^{-5}	1.7×10^{-5}
	10^{48}	2.1×10^{-5}	2.0×10^{-5}
	10^{49}	2.5×10^{-5}	2.2×10^{-5}
10^5	10^{47}	2.2×10^{-4}	2.1×10^{-4}
	10^{48}	2.6×10^{-4}	2.3×10^{-4}
10^6	10^{47}	2.6×10^{-3}	2.3×10^{-3}
	10^{48}	3.0×10^{-3}	2.5×10^{-3}
	10^{49}	3.5×10^{-3}	2.5×10^{-3}

5. EMISSION FROM NGC 7027

In the model calculations we adopted a uniform electron temperature of 10^4 K, an assumption that causes a slight underestimate of the extent of the transition zone where the temperature is falling and recombination is accelerated. For the planetary nebula NGC 7027 detailed models of the density and temperature structure are available, one (model 1) constructed by D. Péquignot & R. B. Gruenwald (1989, private communication) and a second (model 2) by Middlemass (1990). NGC 7027 is the object in which Moorhead et al. (1988) searched for emission lines of HeH^+.

We took the model densities of H^+, He^+, H, and He and used our chemical reaction scheme to compute the equilibrium densities of HeH^+ as a function of distance from the central star.

To calculate the intensities of the HeH^+ emission lines, we adopted an electron impact excitation rate coefficient for the 0–1 vibrational transition of

$$q_{01}(T) = 3.3 \times 10^{-9} \text{ cm}^3\text{ s}^{-1}, \quad (32)$$

which is a compromise between the calculations of Neufeld & Dalgarno (1989) and those of Sarpal, Tennyson, & Morgan (1991). For the rate coefficient for the 0–1 rotational transition we used the values calculated by Flower (1979).

The value of $\int n_e\, n(HeH^+) d\ell$ for model 1 is 4.9×10^{16} cm^{-5}, and for model (2) it is 7.7×10^{16} cm^{-5}. In view of the different densities, the near-agreement of the two models is partly fortuitous. In model 1 the peak density of HeH^+ is 3.9×10^{-3} cm^{-3} at a radial distance of 5.7×10^{16} cm, and in model 2 the peak density is 1.1×10^{-3} cm^{-3} at 8.4×10^{16} cm. The different densities are compensated by the extents of the HeH^+ peaks, which are 1×10^{14} and 3×10^{14} cm for models 1 and 2, respectively. Model 2 is semiempirical, based on the photoionization calculations of Harrington, Monk, & Clegg (1988) and adjusted to match the density structure inferred from the 5 GHz radio map of Scott (1973). Model 1 is a theoretical model at constant pressure. It yields results that are similar to our calculations for a comparable density and a comparable ionizing flux. Both models give satisfactory descriptions of the visible emission nebula.

The predicted intrinsic column emission intensities F_ν of the HeH^+ emission lines for the two models are presented in Table 4. The $P(2)$ line at 3.607 μm lies 0.6 cm^{-1} from the hydrogen recombination line H20-6 and may be unobservable. The $R(0)$ line at 3.364 μm lies on the wing of a strong telluric line of water vapor, but a careful observational study by Moorhead et al. (1988) yielded an upper limit of 3.7×10^{-14} ergs cm^{-2} s^{-1} for the flux. The corresponding column emission intensity depends on the distance to the nebula, but it is within a factor

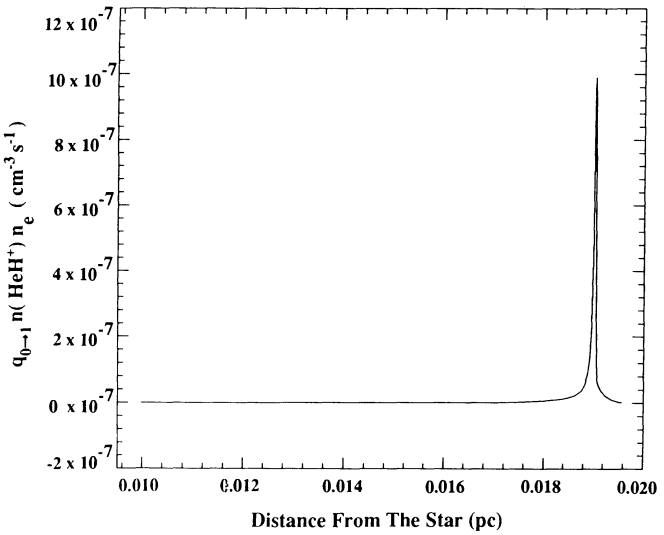

FIG. 7a

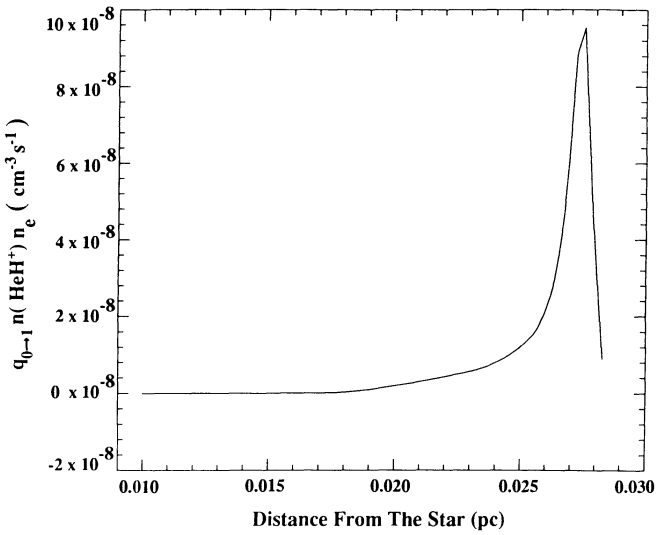

FIG. 7b

FIG. 7.—Distribution of the 0–1 vibrational excitation rate of HeH^+ for (*a*) model 1 and (*b*) model 2

TABLE 4

PREDICTED COLUMN EMISSION INTENSITIES F_ν (ergs cm^{-2} s^{-1})

λ (μm)	Model 1	Model 2
3.364.....	2.5×10^{-5}	3.8×10^{-5}
3.608.....	6.3×10^{-5}	1.0×10^{-4}
149.13.....	2.6×10^{-4}	4.1×10^{-4}

of 2 of 5×10^{-6} ergs cm^{-2} s^{-1} and certainly less than the predicted values, given in Table 4.

The models are inadequate in that they assume spherical symmetry whereas observations indicate a hollow prolate spheroidal shell (Atherton et al. 1979), and observational difficulties may be presented by the nature of the emitting region of the nebula. The distributions of the $R(0)$ line emission intensity with distance from the center of the nebula for the two models are illustrated in Figures 7*a* and 7*b*. Although in the models the maximum emissions occur at the different radial distances of 0.019 and 0.0275 pc for models 1 and 2, respectively, they agree in placing them in a narrow ring just inside the Strömgren radius where some overlap of ionized helium and neutral hydrogen occurs.

Moorhead et al. (1988) used an instrument with an aperture of 8″ centered on the flux maximum through the bandpass (Lowe, Moorhead, & Wehlau 1991), which is smaller than the size of the ionized region. Much of the HeH^+ emission may lie outside the observed volume.

We present predictions of the intensity of the pure rotational line at 149.13 μm in case it becomes possible to search for it.

This work was supported by the National Science Foundation, Division of Astronomical Sciences, under grant AST 89-21939. One of us (C. C.-P.) is grateful to the Italian Ministry for University, Research, and Technology for financial support. We are indebted to D. Péquignot and R. B. Gruenwald and to D. Middlemass and M. Hoare for providing the details of the models of NGC 7027 and permitting us to use them. We are indebted also to J. M. Moorhead and R. P. Lowe for discussions of their observations. J. Yeh was of considerable assistance with the numerical calculations.

REFERENCES

Atherton, P. D., Hicks, T. R., Reay, N. K., Robinson, G. J., Worswick, S. P., & Phillips, J. P. 1979, ApJ, 232, 786
Dalgarno, A., & Lepp, S. 1985, in Astrochemistry, ed. S. P. Tarafdar & M. P. Varshni (Dordrecht: Reidel), 109
Dove, J. E., & Mandy, M. E. 1986, ApJ, 311, L193
Dove, J., Rusk, A. C. M., Cribb, P. H., & Martin, P. G. 1987, ApJ, 318, 379
Draine, B. T., & Lee, H. M. 1984, ApJ, 285, 89
Flower, D. 1979, A&A, 73, 237
Harrington, J. P., Monk, D. J., & Clegg, R. G. S. 1988, MNRAS, 231, 577
Hummer, D., & Seaton, M. J. 1963, MNRAS, 125, 437
———. 1984, MNRAS, 127, 217
Jones, M. E., Barton, S. E., Ellison, G. B., & Ferguson, E. E. 1986, Chem. Phys. Lett., 130, 218
Kossman, H., Schwarzkopf, O., Kämmerling, B., Brau, W., & Schmidt, V. 1989, J. Phys. B, 22, L411
Lepp, S., & Shull, J. M. 1983, ApJ, 270, 578
Lowe, R. P., Moorhead, J. M., & Wehlau, W. H. 1991, ApJ, 368, 195
Michels, H. 1989, in Dissociative Recombination: Theory, Experiment and Applications, ed. B. Mitchell & S. Guberman (Singapore: World Scientific), 97
Middlemass, D. 1990, MNRAS, 244, 294
Moorhead, J. M., Lowe, R. P., Maillard, J. P., Wehalu, W. H., & Bernath, P. F. 1988, ApJ, 326, 899
Neufeld, D. A., & Dalgarno, A. 1989, Phys. Rev. A, 40, 633
O'Neill, S. V., & Reinhardt, W. P. 1978, J. Chem. Phys., 69, 2126
Petrosian, V., & Dana, R. A. 1975, ApJ, 196, 733
Roberge, W. 1990, in Molecular Astrophysics, ed. T. W. Hartquist (Cambridge: Cambridge Univ. Press), 288
Roberge, W., & Dalgarno, A. 1982a, ApJ, 255, 176
———. 1982b, ApJ, 255, 489
Roberge, W., Jones, D., Lepp, S., & Dalgarno, A. 1991, ApJS, 77, 287
Rubin, R. H. 1984, ApJ, 287, 653
Sarazin, C. L. 1977, ApJ, 211, 772
Sarpal, B. K., Tennyson, J., & Morgan, L. A. 1991, J. Phys. B, 24, 1851
Scott, P. F. 1973, MNRAS, 161, 35P
Tielens, A. G. G. M., & de Jong, T. 1979, A&A, 75, 326
Yousif, F. B., & Mitchell, J. B. A. 1989, Phys. Rev. A, 40, 4318
Zygelman, B., & Dalgarno, A. 1990, ApJ, 365, 239